LA-UR -86-3444

CONF-8609131--7
Received by OSTI
NOV 07 1986

Los Alamos National Laboratory is operated by the University of California for the United States Department of Energy under contract W-7405-ENG-36

LA-UR--86-3444

DE87 001958

TITLE *RECENT THEORETICAL RESULTS FOR AN RF-LINAC-DRIVEN XUV FREE-ELECTRON LASER*

AUTHOR(S) *John C. Goldstein*
Brian D. McVey

SUBMITTED TO *Proceedings of the 8th International Free-Electron Laser Conference which was held in Glasgow, Scotland, September 1-5, 1986.*

Los Alamos National Laboratory
Los Alamos, New Mexico 87545

Recent Theoretical Results for an RF-Linac-Driven XUV Free-Electron Laser*

By

John C. Goldstein and Brian D. McVey
Group X-1, MS E531
Los Alamos National Laboratory
Los Alamos, NM 87545
USA

ABSTRACT

We present new theoretical results for the characteristics and performance of an rf-linac-driven XUV free-electron laser. These results fall into two categories: (1) the dependence of the small-signal gain upon the transverse phase-space distribution of the electron beam and the geometry of the optical resonator, and (2) the optical spectral bandwidth. Within (1) we discuss, and present 3-d numerical calculations of, the small-signal gains expected for different phase-space distributions. The gain also varies substantially with the Rayleigh range of the optical resonator. Thus, for maximum small-signal gain, the design of the resonator is coupled to the electron beam characteristics. Within (2), we discuss conditions under which there is a spectral broadening of the optical pulse due to the development of sidebands. The basis of these studies are 1-d finite pulse, and 3-d periodic boundary condition, numerical computer codes.

I. Introduction

In a series of previous theoretical papers [1-4], we have considered the feasibility of operating an XUV (10-100 nm) FEL oscillator driven by an electron beam produced in an rf-linac. These studies have shown that, for

*Work performed under the auspices of, and supported by, the Advanced Energy Projects Division of the Office of Basic Energy Sciences of the U. S. Department of Energy.

modest improvements in electron-beam quality over that presently available from rf-linear accelerators, sufficient small-signal gain (typically several hundred percent) would be available to overcome expected mirror losses in this wavelength range. The small-signal gain would be substantially inhomogeneously broadened due to the relatively large transverse emittance, even with advanced linac designs. However, "high gain" FEL effects and the accompanying optical mode distortion effects [3] due to reduced diffraction at short wavelengths allow substantial broadening without reducing the gain below threshold. It is predicted [3] that such an XUV FEL oscillator could produce light which is several orders of magnitude brighter than that available in the 10-100 nm wavelength range from synchrotron radiation sources.

The present work extends our theoretical considerations in two related but distinct directions: in Part II, the dependence of the small-signal gain upon the form of the electron beam's transverse phase-space distribution for a 12 nm oscillator is presented. In Part III, a discussion of the expected optical spectral bandwidth for a 50 nm oscillator is presented. These two topics are presented separately with a summary and conclusions for each topic at the end of the corresponding section.

II. Small-Signal Gain of an XUV FEL Oscillator For Different Electron-Beam Transverse Phase-Space Distributions.

A. Introduction

Since our previous theoretical calculations [1-3] have shown that the small-signal gain of an rf-linac-driven XUV FEL oscillator is very substantially reduced by the finite transverse emittance of the electron beam (the intrinsic energy spread also contributes to the inhomogeneous broadening and must be carefully controlled), one might expect that the magnitude of the gain would depend on the specific shape of the distribution of electrons in the transverse phase-space of the beam, and not just on the emittance which is a particular moment of the distribution. However, it is difficult to anticipate for the case of a linac what the transverse phase-space distribution, characterized by an emittance, will be because the evolution of the distribution within the accelerator is a transient process which depends upon the initial conditions at the injector and the specific operating configuration of the accelerator sections. This contrasts with the situation in an electron storage

ring in which an equilibrium is reached between synchrotron radiation losses and energy added in the accelerating section. In a storage ring, a Gaussian phase-space density in the transverse variables is thought to be quantitatively correct, but that may not apply to the beam generated in a linac. Hence, in this paper, we investigate the dependence of the small-signal gain upon the form of the transverse phase-space distribution. This work represents an extension to a shorter optical wavelength of the ideas developed in ref. [4]. We choose to explore these ideas for a laser operating at 12 nm since it is expected [5] that a multifaceted rhodium mirror would provide about 60% reflectivity at this wavelength: this implies a laser threshold gain (gain is defined as power output divided by power input) of 2.77 for a two multifaceted mirror resonator.

B. Transverse Phase-space Distributions and Emittance.

Let x, $x' = v_x/c$, y, and $y' = v_y/c$ be the transverse phase-space coordinates of electrons. They are distributed according to a normalized distribution $f(x, x', y, y')$ (let $d\tau = dx\, dx'\, dy\, dy'$):

$$\int f d\tau = 1 \tag{1}$$

The average value of any function g of these coordinates is then given by

$$\langle g \rangle = \int g(x, x', y, y')\, f\, d\tau \tag{2}$$

We define [6] the emittance ϵ as

$$\epsilon = [\epsilon_x \epsilon_y]^{1/2} \tag{3}$$

where

$$\epsilon_x = 4\pi[\langle x^2 \rangle \langle x'^2 \rangle - \langle xx' \rangle^2]^{1/2} \tag{4}$$

$$\epsilon_y = 4\pi[\langle y^2 \rangle \langle y'^2 \rangle - \langle yy' \rangle^2]^{1/2} \tag{5}$$

In this paper we shall assume that

$$\epsilon_x = \epsilon_y = \epsilon \tag{6}$$

The transverse phase-space distribution will be assumed to be a function of the variable B: $f = f(B)$

$$B = (x/\bar{x})^2 + (x'/\bar{x}')^2 + (y/\bar{y}')^2 + (y'/\bar{y}')^2 \tag{7}$$

where $\bar{x}$, $\bar{x}'$, $\bar{y}$, and $\bar{y}'$ are fixed constants. For a parabolic-pole-face untapered wiggler [7], the form of the distribution function inside the wiggler will be the same as outside the wiggler if the following matching conditions hold:

$$\bar{x}' = K_\beta \bar{x} \tag{8}$$

$$\bar{y}' = K_\beta \bar{y} \tag{9}$$

where $K_\beta = (a_w K_w/2\gamma_o)$ is the betatron wavenumber and $a_w = (|e| B_w \lambda_w/2\pi mc^2)$ is the dimensionless wiggler parameter. The distribution will be invariant if the electron energy loss in the wiggler is small, which is the case since we are only interested in small-signal gain values here.

Four different transverse phase-space distribution functions will be considered:

Case 1. Gaussian $f_1 \, d\tau = N \exp(-B) \, d\tau$ (10)

Case 2. "Almost Gaussian" $f_2 \, d\tau = 1.67097 \, N \exp(-B^{1.5}) \, d\tau$ (11)

Case 3. "Almost Uniform" $f_3 \, d\tau = 2.25305 \, N \exp(-B^4) \, d\tau$ (12)

Case 4. Uniform $f_4 \, d\tau = 2N \, d\tau$ for all values (13)

of x, x', y, and y' such that $B \leq 1$.

The normalization factor is $N = (\pi^2 \bar{x} \bar{x}' \bar{y} \bar{y}')^{-1}$. For these four distributions, one can further show that [4]:

Case 1. $\epsilon_x = 2\pi \bar{x} \bar{x}'$ (14)

Case 2. $\epsilon_x = 1.1122\pi \bar{x} \bar{x}'$ (15)

Case 3. $\epsilon_x = 0.687\pi\ \bar{x}\ \bar{x}'$ (16)

Case 4. $\epsilon_x = (2/3)\pi\ \bar{x}\ \bar{x}'$ (17)

Hence, given an electron beam energy γ_o, an emittance value ϵ, and a fixed wiggler design (a_w, K_w), one can uniquely determine the values of all four constants for each of the four distribution functions by using Eqs. (8), (9), (14-17), and (6).

C. Calculated Small-signal Gain Values

We shall compute single pass small-signal gains (rather than the self-consistent resonator solutions) using the three-dimensional free-electron laser simulation program FELEX [8]. The optical beam is initially in the lowest order Gaussian mode of a two-mirror optical resonator and is specified by a Rayleigh range and an optical wavelength. The mode is nominally focused at the center of the wiggler. The finite temporal structure of the electron and light pulses is ignored: gains are single-wavelength time-independent values associated with the peak current of a long electron pulse. All quoted optical gain values have been maximized over a range of optical wavelengths for each Rayleigh range.

Table 1 shows the values of various electron-beam parameters used in the numerical calculations. The parameters of the untapered wiggler magnet are listed in Table 2. Figure 1 shows plots of the numerically calculated small-signal gain, maximized over a range of optical wavelengths near 12 nm, vs. Rayleigh range for each of the four transverse phase-space distribution functions. Note that a two-mirror resonator with 60% reflectivity mirrors [5] has a threshold gain of 2.77. Figure 1 shows that the gain varies with Rayleigh range differently for each of the four cases, and therefore, the maximum gain is attained at different Rayleigh ranges. Case 1, the Gaussian phase-space distribution, clearly yields the largest gain. The other cases are only slightly above threshold, so in obtaining the calculated results below, we used all of the parameter values listed in Tables 1 and 2 except we take a current of 200 A. Figure 2 shows the corresponding gain curves, all of which are now comfortably above threshold. Note that both these figures suggest that the design of the optical resonator (the Rayleigh range) is coupled to the electron-beam phase-space distribution if maximum gain is to be achieved.

Figure 3 shows plots of the partially saturated gain for the same conditions as Fig. 2 except at an initial on-axis light intensity of 5×10^9 w/cm^2. We see from Fig. 3 that the saturated gains peak at about the same Rayleigh range values as did the small-signal gain values of Fig. 2. If this did not occur, the design of the resonator might need to be further complicated.

Figure 4 shows how the gains, maximized over wavelength and Rayleigh range, vary with current at a fixed electron beam brightness. The brightness is given by (I/ϵ_n^2), where ϵ_n is the normalized emittance. One sees from Fig. 4 that the gains are not constant at constant brightness, and therefore are not functions of the brightness only. However, it might be possible to exceed threshold for peak currents less than 200 A at this brightness value of 3.7×10^6 A/cm^2.

D. Summary and Conclusions

We have shown that the magnitude of the small-signal gain depends upon the form of the transverse phase-space distribution function of the electron beam by doing three-dimensional calculations with the code FELEX [8] for four different distribution functions, each of which corresponded to the same transverse emittance. For the examples considered here, the Gaussian distribution gave the largest gain, but that is not necessarily true in all cases [4]. The calculations show that the maximum small-signal gain occurs at different Rayleigh ranges for different transverse phase-space distributions. Therefore, this couples the design of the optical resonator to the electron-beam properties. We found that a current of 200A is needed at a normalized emittance $\epsilon_n = 23.4\pi \times 10^{-4}$cm rad for peak gain values of all of the distributions considered here to comfortably exceed the threshold value of 2.77 expected [5] for a resonator made with two multifaceted rhodium mirrors for use with an optical wavelength of about 12 nm. A discussion of similar calculations in terms of the shape of the corresponding effective energy distribution, and the transverse spatial overlap between the optical mode and the electron beam, is given in ref. [4]. We also showed that peak values of saturated gain occur for nearly the same Rayleigh ranges as maximized the small-signal gains. It was demonstrated that the small-signal gain varies with current at a fixed electron-beam brightness, and the variation is different for different phase-space distributions.

III. The Optical Spectrum of an Rf-Linac-Driven XUV FEL Oscillator.

A. Introduction

If radiation from an XUV FEL oscillator is to be used for spectroscopic studies, it is essential to know what the spectral width of the light will be. Here we present numerical calculations of the spectral properties expected of a 50 nm FEL oscillator. In particular, we show that sideband generation [9], [10] will occur with an accompanying increase in both power and spectral bandwidth. We show how to avoid sidebands by (1) increasing the optical resonator output coupling and (2) operating at a finite cavity length detuning. Both methods avoid sideband generation by reducing the intracavity optical power.

B. Calculated Spectral Properties

The onset of the sideband instabillity [9] in a FEL oscillator occurs when the synchrotron length L_s is comparable to the length of the wiggler L_w:

$$L_s = [(2\gamma_0^4 \lambda_s^2)/(a_w(1 + 0.5\ a_w^2)a_s)]^{1/2} \qquad (18)$$

where $a_s = |e|\ E_s/(mc^2 K_s)$ and E_s is the amplitude of the optical field. For a uniform wiggler, the optical power saturates when the electrons execute a partial synchrotron oscillation. The sideband instability is a potential problem if very narrow bandwidth light is needed for spectroscopic applications.

In this work, the sideband instability is controlled by reducing the optical power level in the FEL oscillator (hence one has $L_s >> L_w$). This is accomplished by: (1) increasing the output coupling of the optical resonator, and (2) optical cavity length detuning. The 1-d time-dependent computer code FELP is used to perform simulations to investigate the optical spectrum of the oscillator. FELP (FEL Pulse) models the longitudinal micropulse structure of the electron bunch from an rf-linac: in this work, the bunch length is taken to be 20 ps. In the periodic [11] and pulse [9] approximations, FELP simulates the sideband instability including an effective energy spread [2], [4] which models the electron beam transverse emittance. Periodic simulations were used to determine the effect of output coupling on the optical spectrum. Pulse simulations were made for the cavity length detuning curves. One-dimensional gains are calibrated to three-dimensional results by adjusting the

optical beam size via the Rayleigh range. The parameter values used in the calculations are given in Table 3.

Figure (5a) shows the calculated optical power vs. the number of passes through the optical cavity, and Fig. (5b) shows the corresponding gain per pass. The small plateau in Fig. (5a) and the steep drop in Fig. (5b) near pass 50 mark the onset of significant sideband modulation of the laser light. Note from Fig. (5a) that the power increases substantially after this onset. Table 4 shows the effect of increasing the output coupling upon the intracavity power and spectral bandwidth. If 90% of the total optical power is contained within a wavelength interval of width $\Delta\lambda$ which is centered at the wavelength λ at which the spectral density is maximum, the bandwidth is defined to be $\Delta\lambda/\lambda$. If a power P_{in} is incident on the entrance to the wiggler, P_{in} G is the power output from the wiggler, where G is the gain. After making one round trip in the cavity, the power incident upon the wiggler entrance on the beginning of the next pass is (1-cavity loss) x P_{in} x G. The excess small-signal gain SSG is then given by

$$SSG = (1\text{-cavity loss}) \times G - 1 \qquad (19)$$

Note that "cavity loss" includes losses due to mirror reflectivity as well as output coupling. Table 4 shows that increasing the output coupling ("cavity loss") reduces the net small-signal gain SSG, the equilibrium cavity power, and also the bandwidth. These results depend somewhat upon the model of spontaneous emission in the calculations, and that model may be refined further in future work.

The variation of the bandwidth with pass number is shown in Fig. (6a) for zero cavity length detuning and in Fig. (6b) for -50μm cavity length detuning. One sees that at -50μm, the bandwidth equilibrates at a low level due to the absence of sidebands. Figure (7a) shows the calculated desynchronism curve, while Fig. (7b) shows the associated optical bandwidth vs. cavity length detuning.

C. Summary and Conclusions

We have shown by numerical calculations that the sideband instability [9], [10] is a potential problem in an XUV FEL driven by an rf-linear accelerator, if very narrow optical bandwidths are required for spectroscopic

applications of the generated light. Control of sideband generation and the associated spectral broadening is possible by (1) increasing the output coupling of the optical resonator or by (2) cavity length detuning. Both of these methods reduce the steady state intracavity power. For an rf-linac-driven FEL oscillator operating at a wavelength of 50 nm, we have calculated that, with sidebands allowed to grow, an intracavity power of tens of megawatts and an optical bandwidth of about 1% is to be expected. With the sidebands suppressed, the expected intracavity power is a few megawatts and the bandwidth is $\leq$ 0.1%.

Table 1: Standard Parameter Values for the Electron Beam

peak current I	150
electron relativistic factor E/mc^2	$\gamma_0 = 1045.62$ (534.3 MeV)
transverse emittance ϵ	7.0306×10^{-4} cm rad
normalized emittance $\epsilon_n = \gamma_0 \epsilon$	$23.4\pi \times 10^{-4}$ cm rad
betatron wavelength $\lambda_\beta = 2\pi/K_\beta$	2.9875×10^{3} cm
fractional intrinsic energy spread $\Delta\gamma/\gamma_0$	1×10^{-3}

Table 2: Untapered Wiggler Parameter Values

wavelength, λ_w	1.6 cm
peak magnetic field, B_w	0.75 T
dimensionless wiggler parameter a_w	1.12
full gap	0.4 cm
length	1.2×10^3 cm
magnet material	SmCo
parabolic-pole-face with equal focusing in x and y	

Table 3: FEL Oscillator Parameter Values for Spectral Studies

optical beam : λ = 50 nm

electron beam: I = 150 A, γ_o = 511.5, $\Delta\gamma/\gamma_o$ = .2%, ϵ_n = $40\pi \times 10^{-4}$ cm rad

wiggler : L_w = 800 cm, λ_w = 1.6 cm, B_w = .75 T, parabolic-pole-face with equal focusing in x and y

small-signal gain: 5.2

average power: 10^{-4} x peak power

Table 4: Increased output coupling reduces the optical bandwidth

Cavity Loss (%)	SSG (%)	Cavity Power (MW)	Bandwidth (%)
59	105	60	.9
64	80	37	.7
69	60	20	.6
74	32	8	.4
77	18	2.5	.06
79	8	1.1	.06

Figure Captions:

Fig. 1 Small-signal gain vs. Rayleigh range (for λ = 12 nm) for standard parameter values for four different phase-space distribution functions.

Fig. 2 Small-signal gain vs. Rayleigh range for I = 200A and other standard parameter values.

Fig. 3 Partially saturated gain vs. Rayleigh range.

Fig. 4 Maximum small-signal gain vs. peak current at fixed electron-beam brightness.

Fig. 5a Optical power vs. pass number.

Fig. 5b Gain vs. pass number.

Fig. 6a Bandwidth vs. pass number at zero cavity length detuning.

Fig. 6b Bandwidth vs. pass number at -50μm cavity length detuning.

Fig. 7a Intracavity power vs. cavity length detuning.

Fig. 7b Optical spectral bandwidth vs. cavity length detuning.

References

1. B. E. Newnam, J. C. Goldstein, J. S. Fraser, and R. K. Cooper, in Free Electron Generation of Extreme Ultraviolet Coherent Radiation, AIP Conference Proceedings No. 118, J. M. J. Madey and C. Pellegrini, Eds. (American Institute of Physics, N.Y., 1984), p. 190.

2. J. C. Goldstein, B. E. Newnam, R. K. Cooper, and J. C. Comly, Jr., in Laser Techniques in the Extreme Ultraviolet, AIP Conference Proceedings No. 119, S. E. Harris and T. B. Lucatorto, Eds. (American Institute of Physics, N.Y., 1984), p. 293.

3. J. C. Goldstein, B. D. McVey, and B. E. Newnam, in International Conference on Insertion Devices for Synchrotron Sources, R. Tatchyn and I. Lindau, Eds., Proc. SPIE 582, pp. 350-360 (1986).

4. J. C. Goldstein, B. D. McVey, and B. E. Newnam, in Short Wavelength Coherent Radiation: Generation and Application, AIP Conference Proceedings No. 147, D. T. Attwood and J. Bokor, Eds. (American Institute of Physics, N.Y., 1986), p. 275.

5. B. E. Newnam in Laser Induced Damage in Optical Materials: 1985, NBS Spec. Publ., H. E. Bennett, A. H. Guenther, D. Milam, and B. E. Newnam, Eds., to be published (1986).

6. J. S. Fraser, R. L. Sheffield, E. R. Gray, and G. W. Rodenz, IEEE Trans. on Nucl. Sci., NS-32, 1791 (1985).

7. E. T. Scharlemann, J. Appl. Phys. 58, 2154 (1985).

8. B. D. McVey in Proceedings of the Seventh International Conference on Free Electron Lasers, E. T. Scharlemann and D. Prosnitz, Eds., Nucl. Inst. and Meth. in Phys. Research A250, p. 449 (1986).

9. J. C. Goldstein, in Free-Electron Generators of Coherent Radiation, Proc. SPIE 435, C. A. Brau, S. F. Jacobs, and M. O. Scully, Eds., p. 2 (1984).

10. R. W. Warren, B. E. Newnam, and J. C. Goldstein, IEEE J. Quant. Electron. QE-21, p. 882 (1985).

11. W. B. Colson, in Free-Electron Generators of Coherent Radiation, Proc. SPIE 435, C. A. Brau, S. F. Jacobs, and M. O. Scully, Eds., p. 290 (1984).

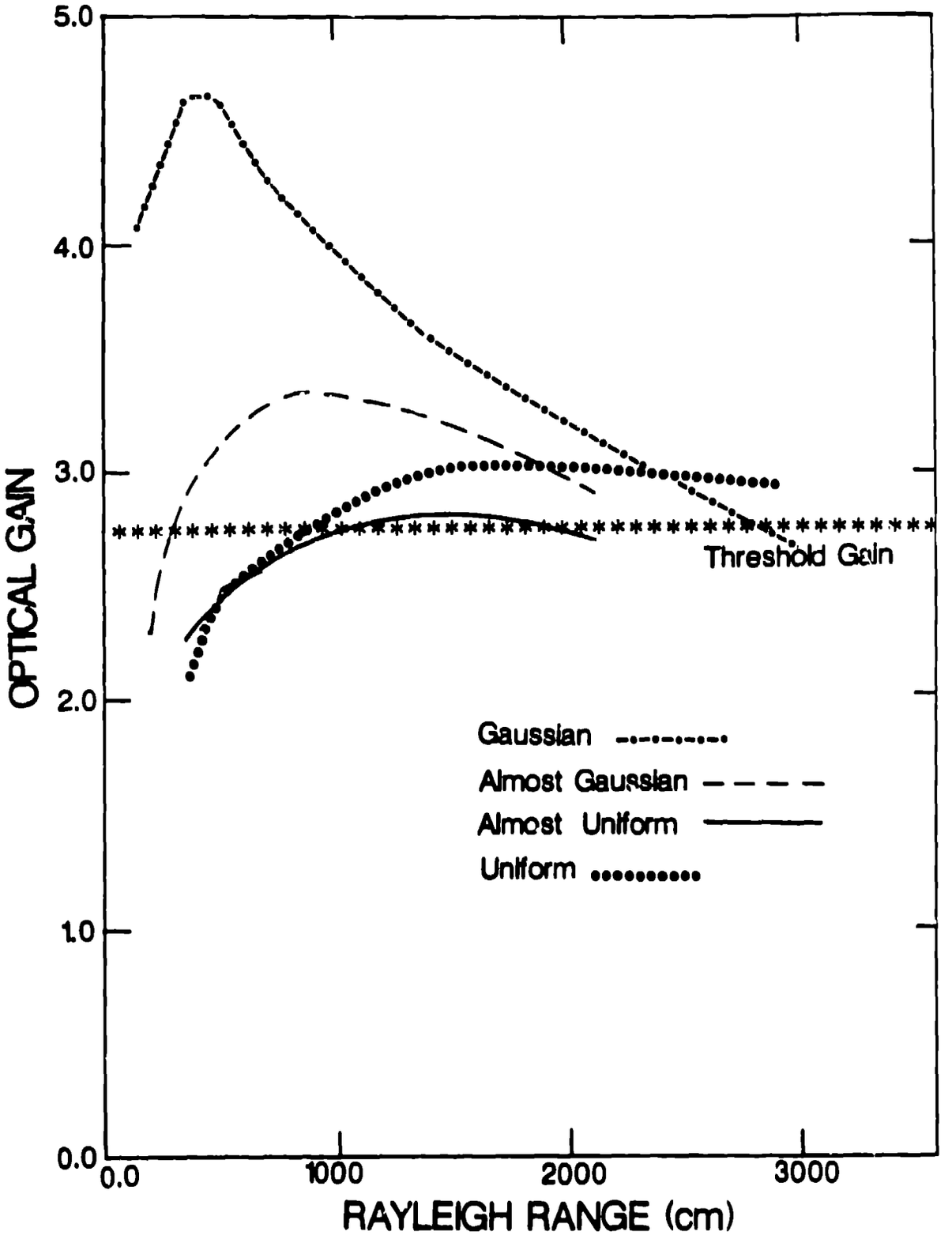
5.0
4.0
3.0
2.0
1.0
0.0
OPTICAL GAIN
0.0
1000
2000
3000
RAYLEIGH RANGE (cm)
Threshold Gain
Gaussian
Almost Gaussian
Almost Uniform
Uniform

FIGURE 1

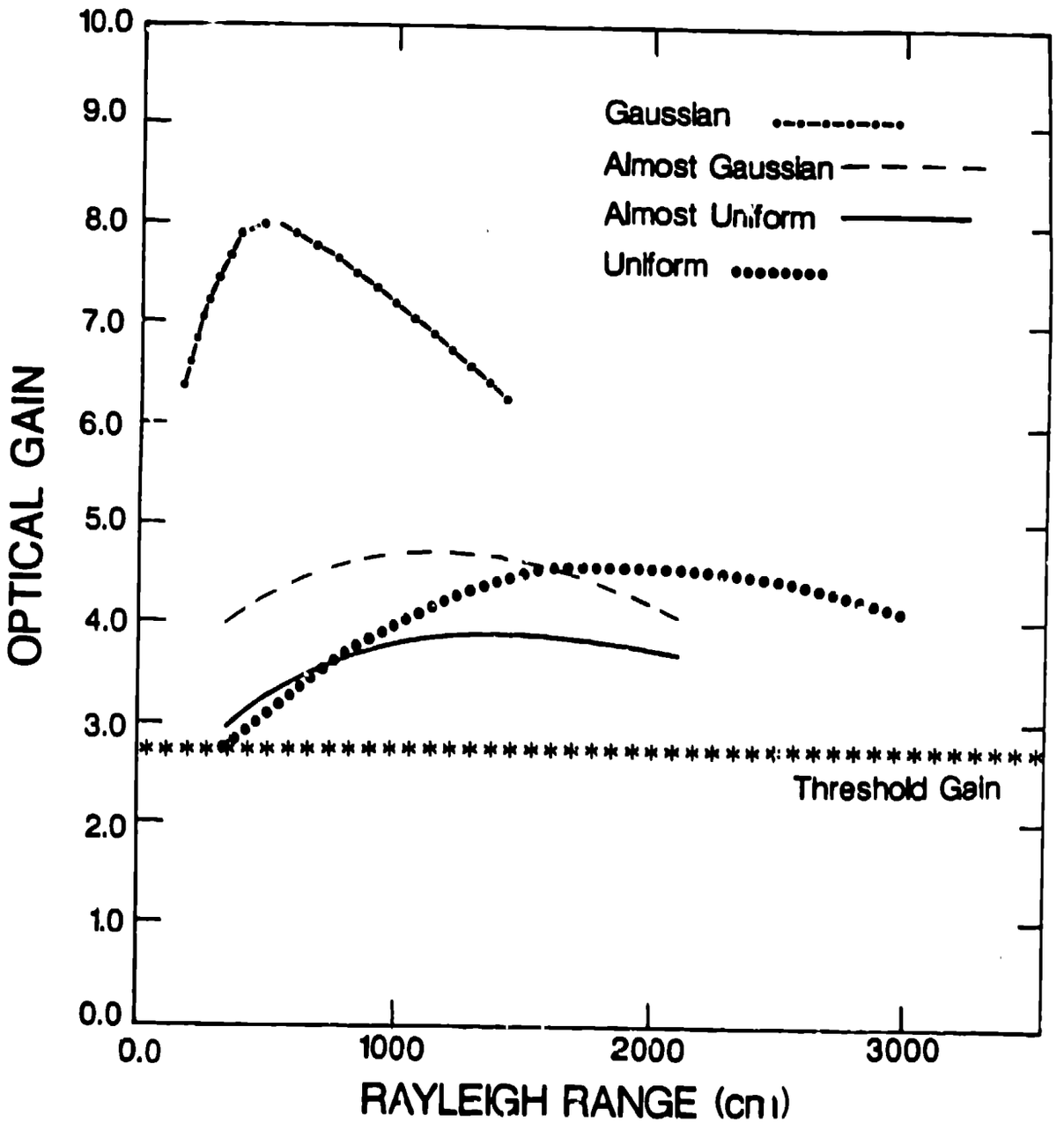
10.0
9.0
8.0
7.0
6.0
5.0
4.0
3.0
2.0
1.0
0.0
OPTICAL GAIN
Gaussian
Almost Gaussian
Almost Uniform
Uniform
Threshold Gain
0.0
1000
2000
3000
RAYLEIGH RANGE (cm)

FIGURE 2

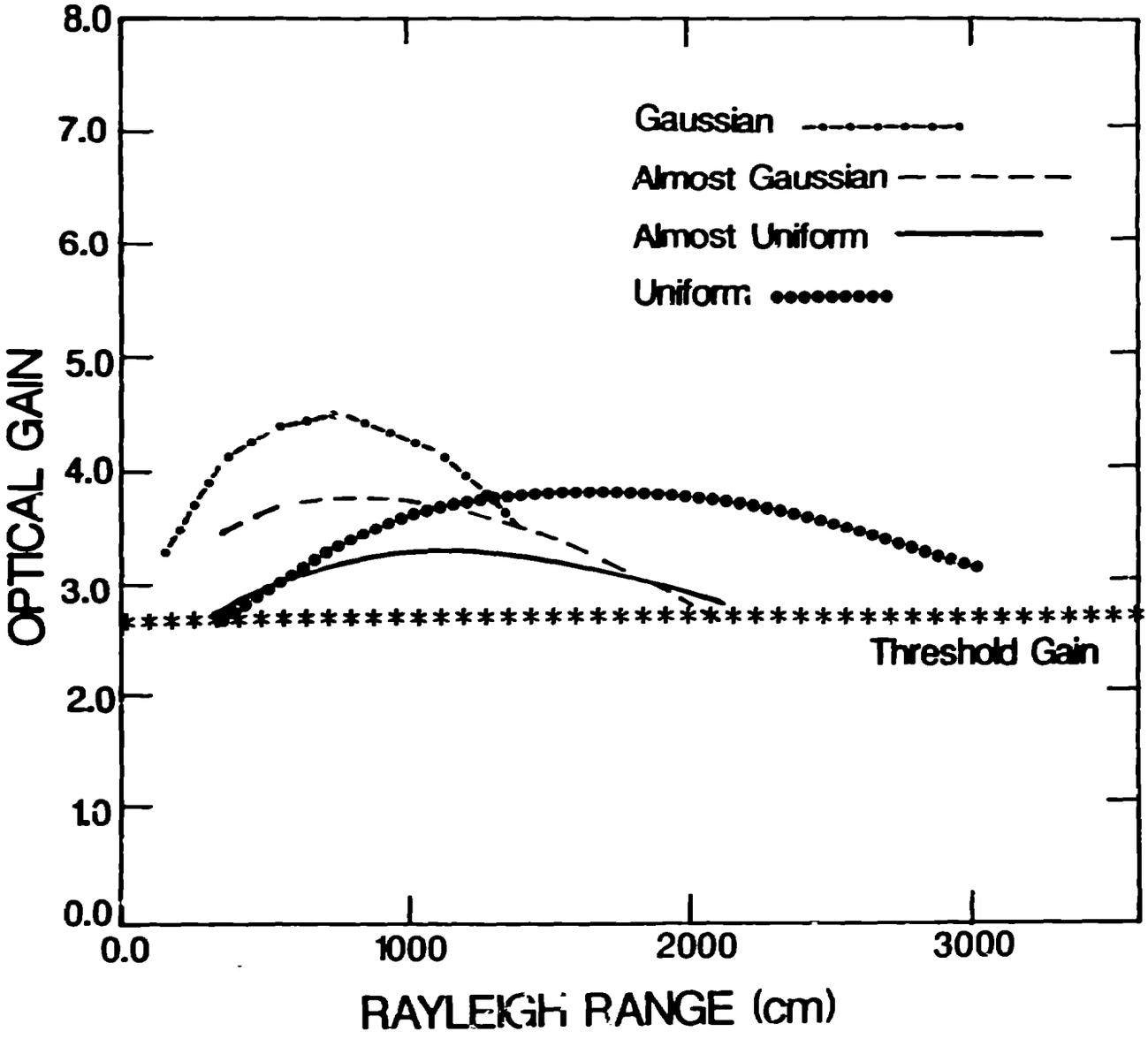
8.0
7.0
6.0
5.0
4.0
3.0
2.0
1.0
0.0
OPTICAL GAIN
Gaussian
Almost Gaussian
Almost Uniform
Uniform
Threshold Gain
0.0
1000
2000
3000
RAYLEIGH RANGE (cm)

FIGURE 3

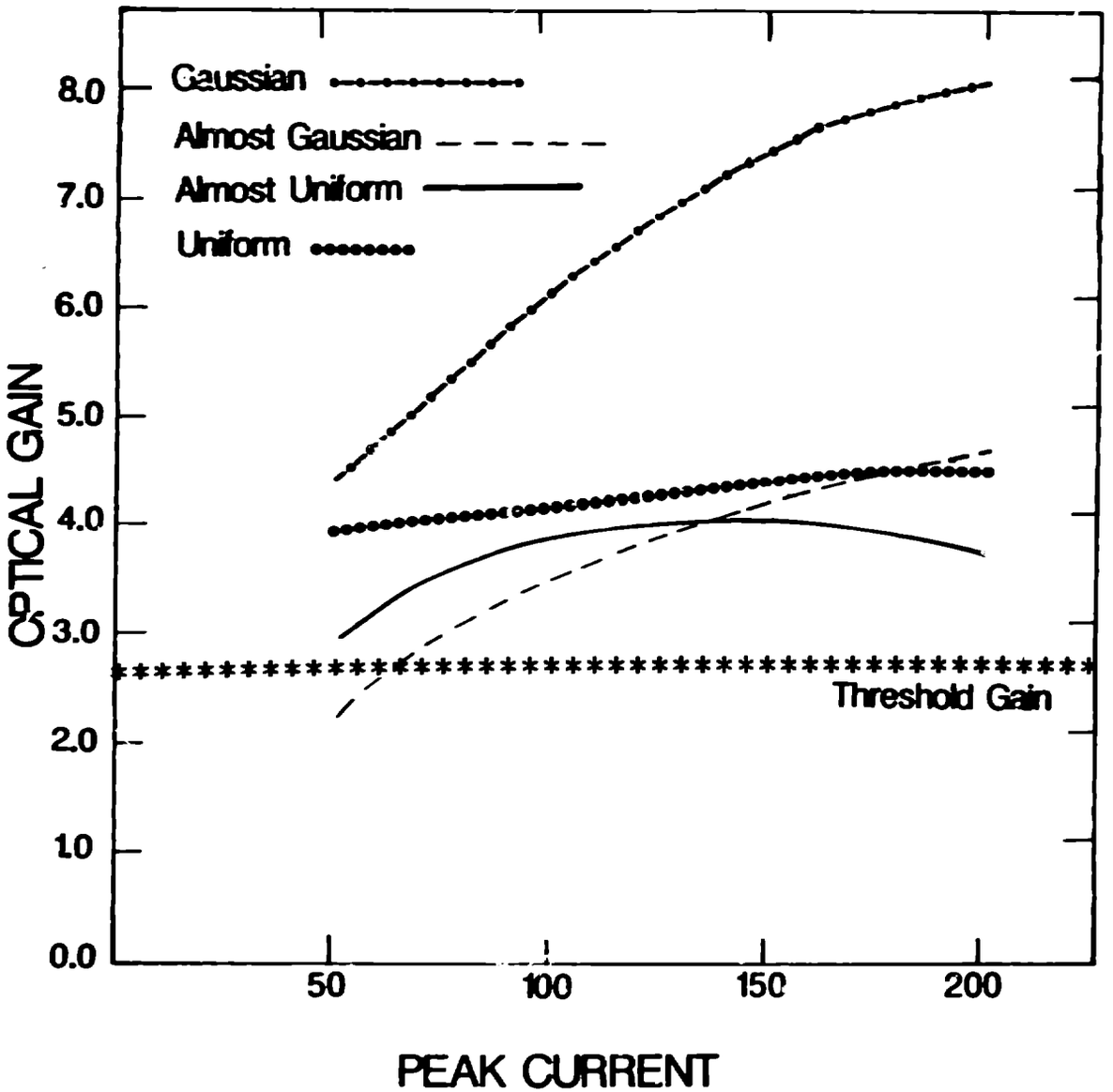
Gaussian
Almost Gaussian
Almost Uniform
Uniform
Threshold Gain
OPTICAL GAIN
8.0
7.0
6.0
5.0
4.0
3.0
2.0
1.0
0.0
50
100
150
200
PEAK CURRENT

FIGURE 4

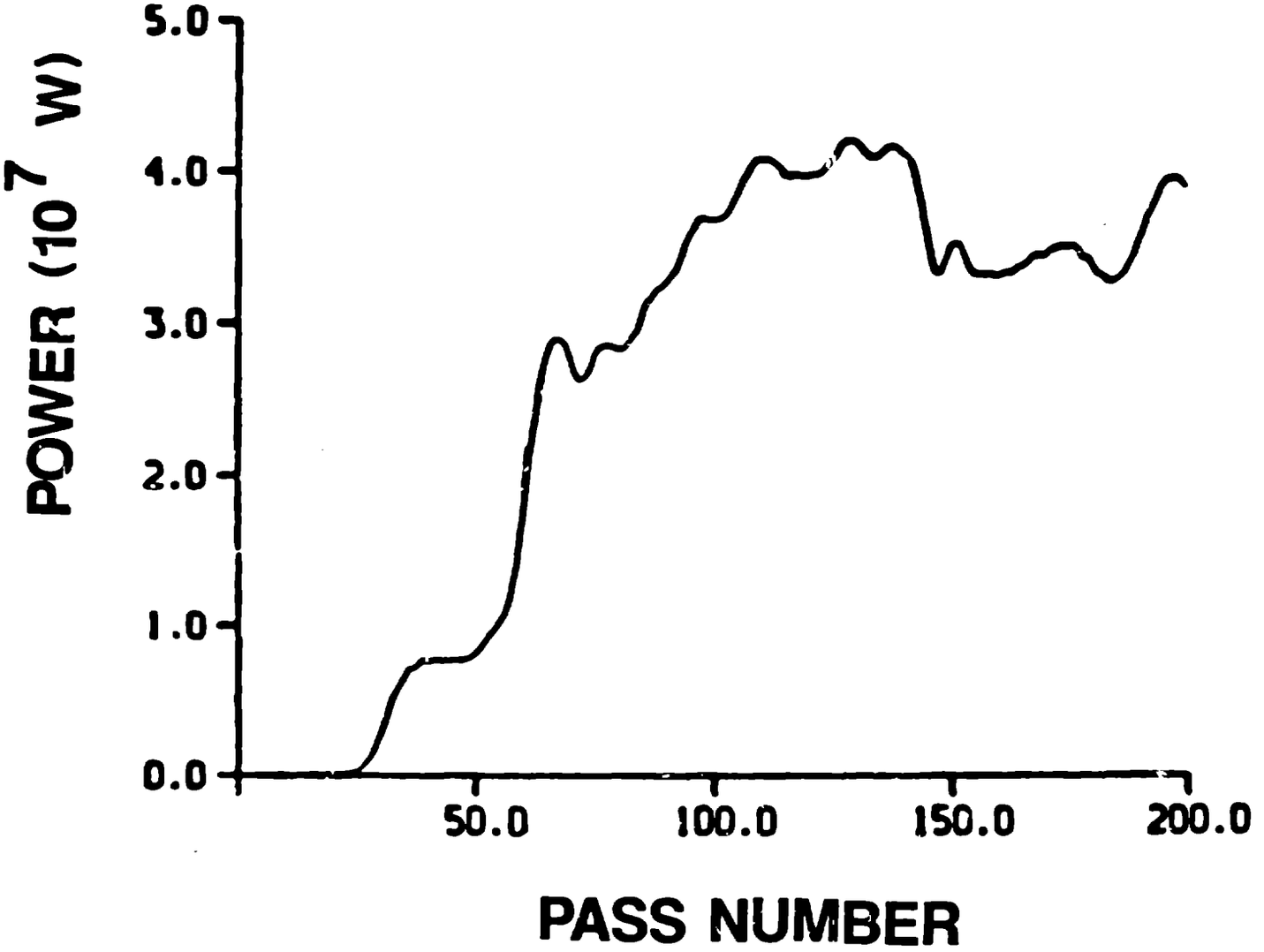

FIGURE 5a

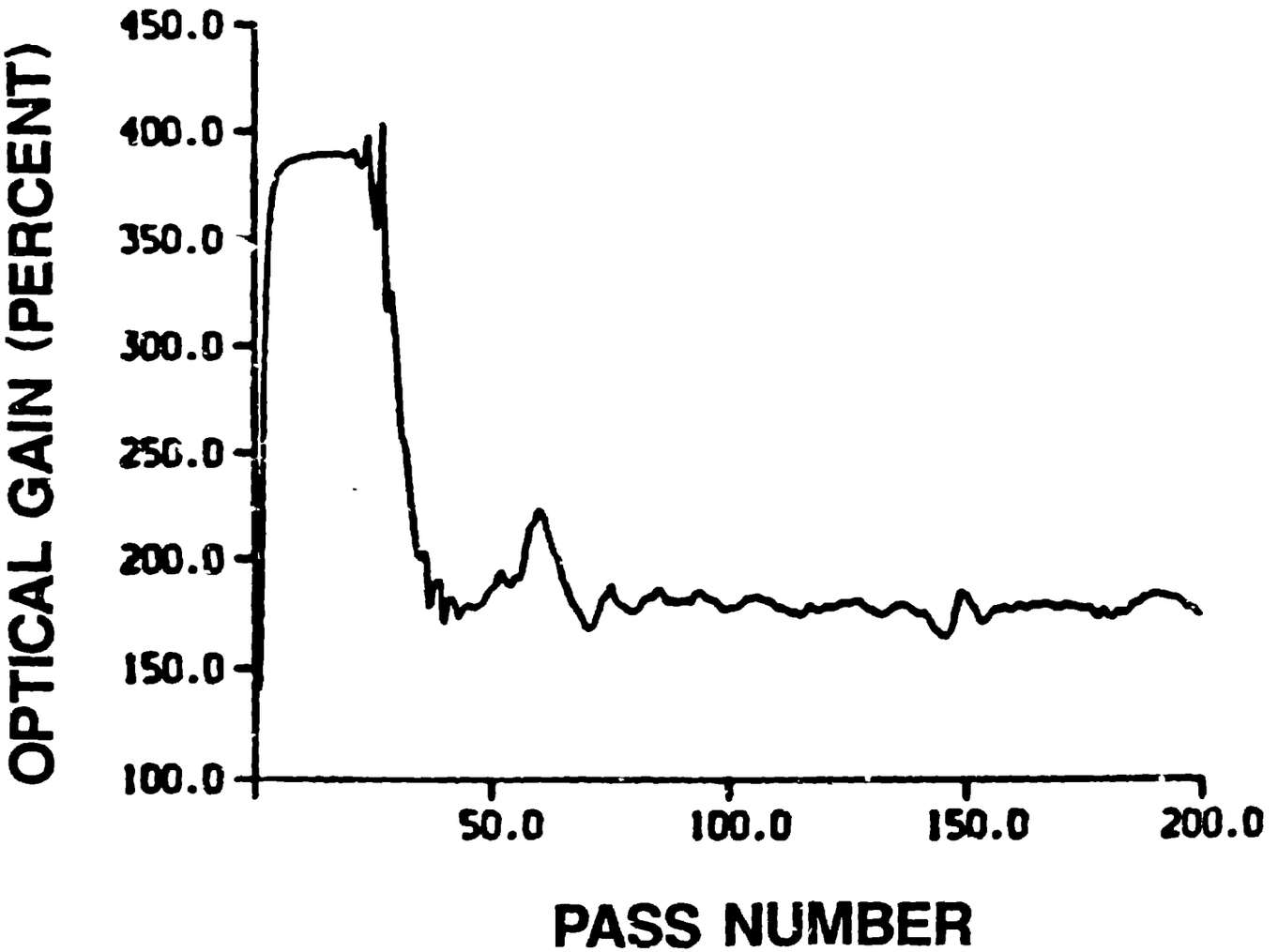
OPTICAL GAIN (PERCENT)
450.0
400.0
350.0
300.0
250.0
200.0
150.0
100.0
50.0
100.0
150.0
200.0
PASS NUMBER

FIGURE 5b

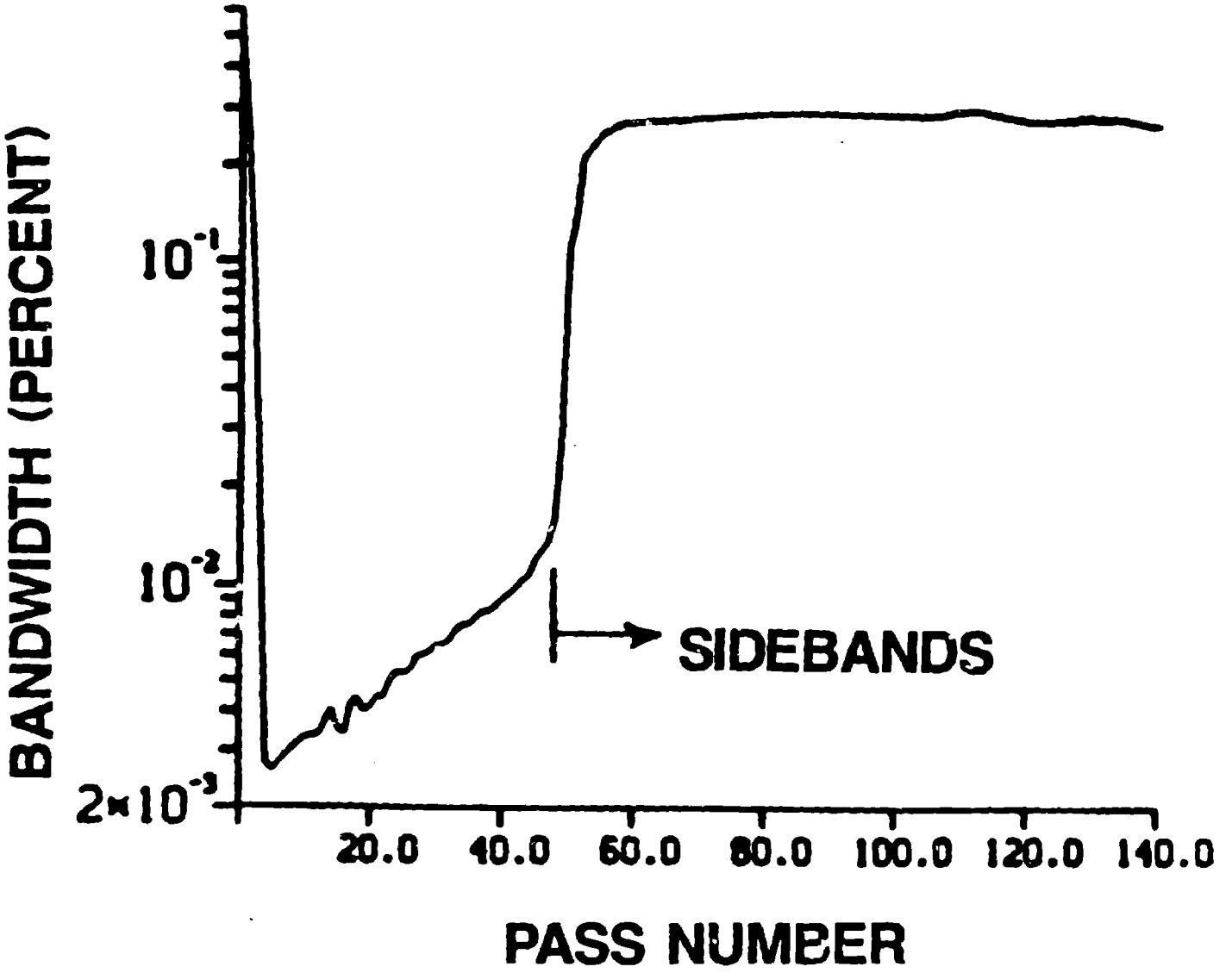
BANDWIDTH (PERCENT)
10^{-2}
10^{-2}
2×10^{-3}
SIDEBANDS
20.0
40.0
60.0
80.0
100.0
120.0
140.0
PASS NUMBER

FIGURE 6a

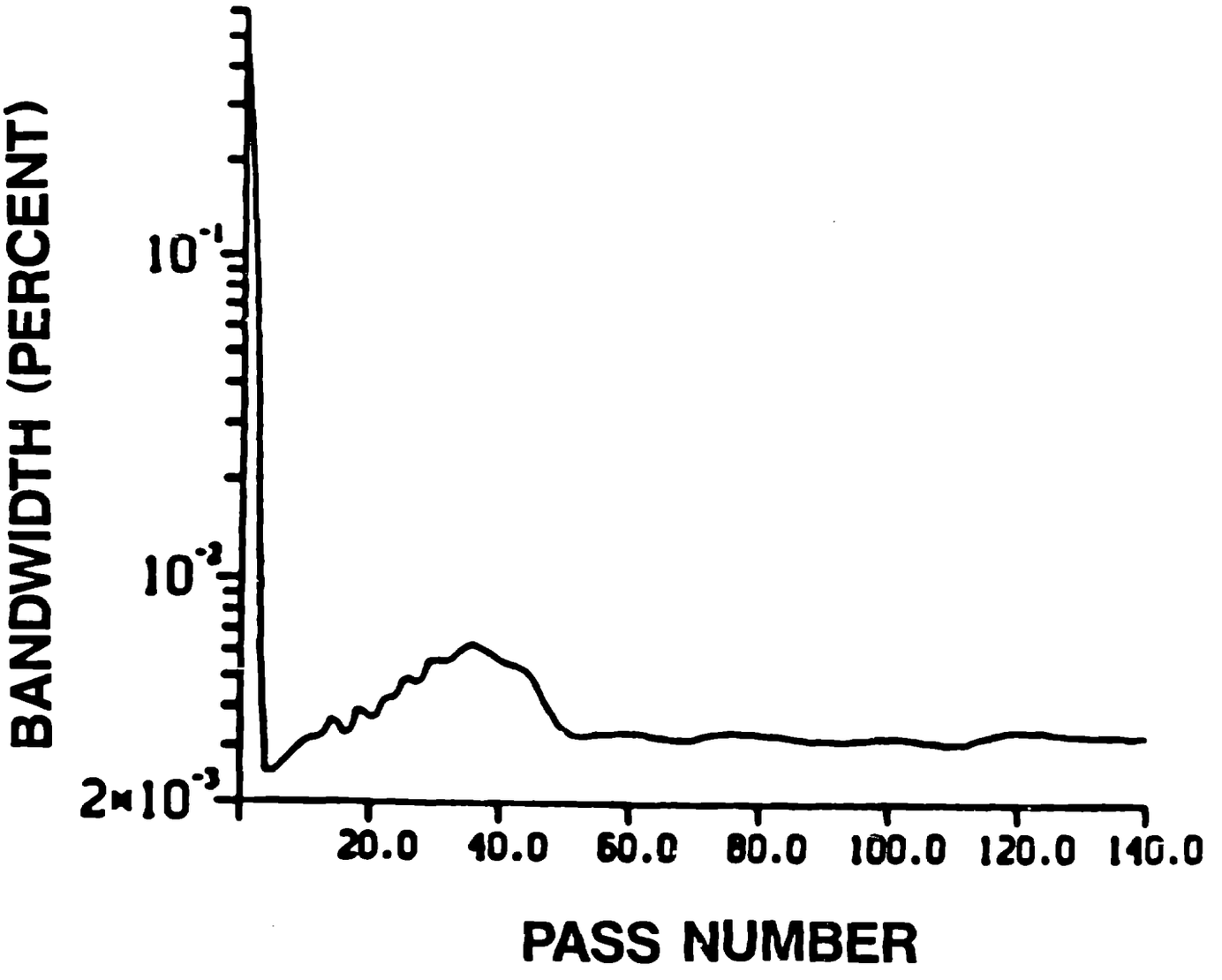
BANDWIDTH (PERCENT)
10^{-1}
10^{-2}
2×10^{-3}
20.0
40.0
60.0
80.0
100.0
120.0
140.0
PASS NUMBER

FIGURE 6b

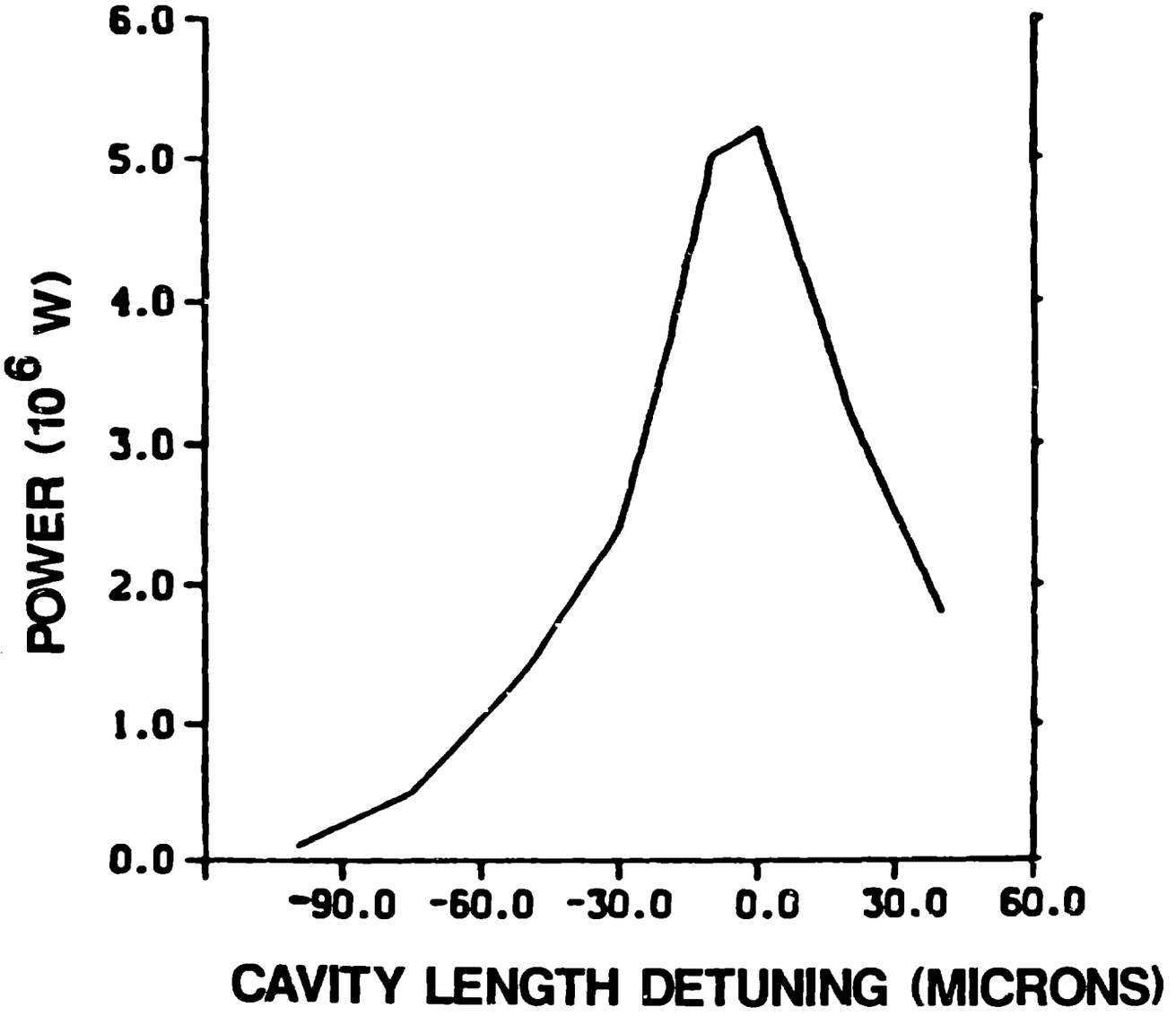
6.0
5.0
4.0
3.0
2.0
1.0
0.0
POWER (10^6 W)
-90.0
-60.0
-30.0
0.0
30.0
60.0
CAVITY LENGTH DETUNING (MICRONS)

FIGURE 7a

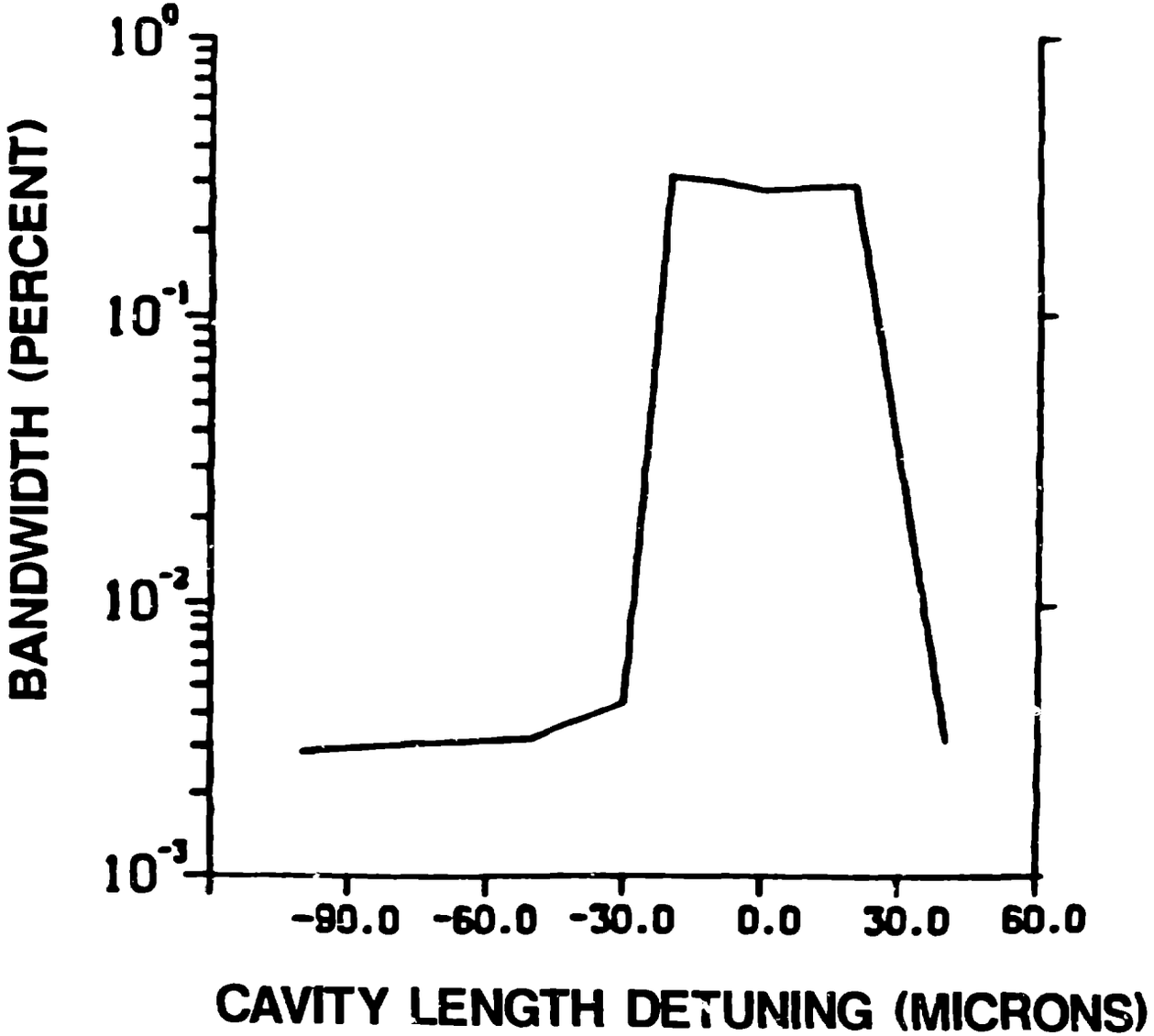
BANDWIDTH (PERCENT)
10^0
10^-1
10^-2
10^-3
-90.0
-60.0
-30.0
0.0
30.0
60.0
CAVITY LENGTH DETUNING (MICRONS)

FIGURE 7b